Aromaticity Changes along the Lowest-Triplet-State Path for C=C Bond Rotation of Annulenyl-Substituted Olefins Probed by the Electron Localization Function

ARTICLE *in* THE JOURNAL OF PHYSICAL CHEMISTRY A · OCTOBER 2009

Impact Factor: 2.69 · DOI: 10.1021/jp904335j · Source: PubMed

Aromaticity Changes along the Lowest-Triplet-State Path for C=C Bond Rotation of Annulenyl-Substituted Olefins Probed by the Electron Localization Function

Sébastien Villaume and Henrik Ottosson*

Department of Biochemistry and Organic Chemistry, Box 576, Uppsala University, 751 23 Uppsala, Sweden

Received: May 9, 2009; Revised Manuscript Received: September 3, 2009

The π-contribution to the electron localization function (ELF_π) was used to analyze changes in the aromaticity of annulenyl-substituted olefins in their lowest triplet state (T_1) when the structure around the olefin C=C bond is twisted from planar to a structure ($^3p^*$) at which the planes of the two RR′C units are perpendicular. The ring closure bifurcation value and the range in the bifurcation values of the ELF_π basins serve as (anti)aromaticity indicators directly linked to the electronic structure. Both Hückel's $4n + 2$ π-electron rule for aromaticity in the singlet ground state (S_0) and Baird's $4n$ π-electron rule for aromaticity in the lowest $\pi\pi^*$ triplet state are applied. Three olefins with S_0 aromatic (T_1 antiaromatic) substituents and four olefins with T_1 aromatic (S_0 antiaromatic) substituents were studied using the ELF_π topology at the OLYP/6-311G(d,p) density functional theory level. The changes in the substituent ELF_π bifurcation values upon rotation about the olefin bond in the T_1 state reveal that aromatic character is recovered for the first three olefins and that it is reduced for the latter ones. These changes in aromatic character are reflected in the shapes of the T_1 potential energy surfaces as a twist away from planar structures in olefins with T_1 antiaromatic substituents is energetically favorable, but that in olefins with T_1 aromatic substituents is unfavorable. Hence, aromaticity change is a driver for a photochemical reaction as for many ground-state reactions.

Introduction

Aromaticity is a key property for chemistry in the electronic ground state,[1,2] and chemical reactions in which aromaticity is gained are mostly very favorable processes. However, despite the fact that the rule for (anti)aromaticity in the lowest $\pi\pi^*$ triplet excited state (T_1) of annulenes was derived by Baird already in 1972,[3] it has essentially never been applied to rationalize photochemical reactions. This rule says that annulenes with $4n$ π-electrons are aromatic in the T_1 state whereas those with $4n + 2$ π-electrons are antiaromatic, i.e., opposite Hückel's rule for ground-state aromaticity.

The validity of Baird's rule was verified by Schleyer and coworkers through high-level quantum chemical calculations of aromatic stabilization energies (ASEs) and nucleus-independent chemical shifts (NICSs) of a set of annulenes in their T_1 states.[4] Recently, we applied the π-contribution to the electron localization function (ELF_π), and in particular analyzed the range in the bifurcation values of the basins of the ELF_π as an (anti)aromaticity indicator directly linked to electronic structure.[5] This analysis supported Baird's postulation of triplet-state aromaticity of annulenes with $4n$ π-electrons. Soncini and Fowler also deduced that the aromaticity and antiaromaticity rules can be generalized to higher spin states so that annulenes with $4n + 2$ π-electrons in states of even total spin (singlet, quintet, etc.) and annulenes with $4n$ π-electrons in states of odd total spin (triplet, septet, etc.) should be aromatic.[6] Using valence bond theory, Haas and Zilberg showed that the lowest singlet excited state (S_1) of annulenes with $4n$ π-electrons should be aromatic,[7] and Garavelli et al. revealed that cyclooctatetraene at the CASSCF level adopts a D_{8h} (aromatic) structure in the S_1 state.[8] Also most recently, Karadakov calculated NICSs, proton shieldings, and magnetic susceptibilities at the CASSCF level to confirm that the excited-state (anti)aromaticity concept is indeed extendable to the S_1 states of cyclobutadiene, benzene, and cyclooctatetraene as these molecules at their most symmetric structures display the same (anti)aromaticity trends as in their T_1 states,[9,10] although cyclobutadiene in its S_1 state has been concluded to prefer a rhomboid D_{2h} symmetric structure rather than the square structure.[11]

Baird's rule should be applied to rationalize excited-state properties and photochemical reactions, and we have earlier used it to explain the polarity reversal of fulvenes in their T_1 states, and fulvalenes and azulene in their lowest quintet state (Qu_1), when compared to S_0.[12] This finding could be applied to design substituted fulvenes with widely variable T_1 and S_1 excitation energies.[13] Using DFT, we further computed the geometry and spin density distributions of olefins that *Z*/*E*-isomerize in their lowest triplet states, and it was found that the structure on the T_1 potential energy surface (PES) for which geometry and spin density suggest the highest aromatic character is of lowest energy.[14] In a subsequent study we found that the differences in the values of geometric and magnetic aromaticity measures (harmonic oscillator model of aromaticity (HOMA)[15] and NICS) between planar and perpendicularly twisted structures of simple annulenyl-substituted olefins vary in a zigzag manner when the number of π-electrons of the substituents increases in steps of 2.[16] However, the HOMA and NICS (anti)aromaticity measures applied in our previous study only indirectly link to the electronic structure of the substituted olefins. Measures that link directly to the electronic structure are instead desirable, as recently found by Sola and co-workers when they examined the performance of 10 indicators/measures through 15 aromaticity tests.[17] It was observed that electronically based aromaticity indices, such as the multicenter indices I_{ring}, I_{NG}, MCI, and I_{NB} as well as $FLU^{1/2}$ and PDI,[18−23] display better general performances than both magnetically and geometrically based indices.

Topological analysis of the ELF, and in particular ELF_π, can be used to directly link aromaticity to electronic structure, and

10.1021/jp904335j CCC: $40.75
Published on Web 10/02/2009

SCHEME 1

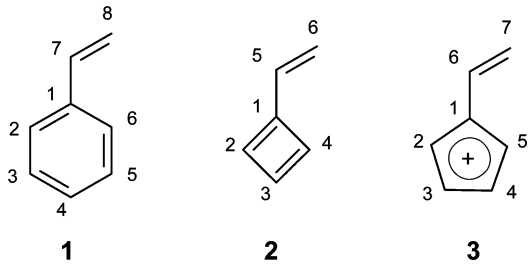

1 **2** **3**

it was first exploited by Santos et al., and later by Malrieu et al., and us.[5,24−26] The ELF_π describes the kinetic energy destabilization due to Pauli repulsion between same-spin π-electrons, and it takes values in the range $0 \leq ELF_\pi \leq 1$. The function is defined so that values close to 1 reveal localization of a π-electron pair, whereas a value close to 0 indicates strong Pauli repulsion between same-spin electrons and is found in regions separating electron pairs. We applied the range in the bifurcation values of the basins of the ELF_π ($\Delta BV(ELF_\pi)$) and the ring closure bifurcation value ($RCBV(ELF_\pi)$) as aromaticity indicators in all-C rings. Aromatic all-C systems should have small $\Delta BV(ELF_\pi)$, ideally 0, and the $RCBV(ELF_\pi)$ should be relatively high, proposed to be above 0.70. In contrast, antiaromatic annulenes have large $\Delta BV(ELF_\pi)$, revealing strong localization of π-electron pairs to distinct CC bonds, and their $RCBV(ELF_\pi)$ values are very low (typically below 0.2). We used these ELF_π properties to characterize a set of annulenes as aromatic or antiaromatic in their S_0 and T_1 states, respectively. At this point it should be remarked that the ELF_π-based properties are indicators of (anti)aromaticity rather than precise measures as they depend on the number of electrons in the ring as well as on the ring size. The ELF_π properties can therefore not be used to assess the exact degree of aromaticity, except in relative terms in a series of compounds which are structurally related.

Ample experimental and computational data exist on the triplet-state isomerization of styrenes, stilbenes, and other olefins with aromatic substituents,[27] but to our knowledge only one study of the T_1-state *Z*/*E*-isomerization of an olefin with a $4n$ π-electron substituent has been reported.[28] Anger et al. found bisstyrylcyclooctatetraene to isomerize very inefficiently, a fact that likely can be linked to loss of the T_1 aromaticity of the cyclooctatetraenyl (COT) ring along the isomerization route. For further design of olefins as, e.g., optical switches, it is important to obtain a precise understanding of the aromaticity changes along the excited-state *Z*/*E*-isomerization path and to link this to the electronic structure.

Herein, we exploit the ELF_π properties to examine how the aromaticity of the annulenyl substituent of an olefin in the T_1 state changes as one twists about the C═C bond from the planar structure to a structure ($^3p^*$) at which the planes of the two CRR′ units of the olefin stand perpendicular to each other. This would verify that a change in triplet-state (anti)aromaticity is indeed a driver for photochemical *Z*/*E*-isomerizations. The change in $\Delta BV(ELF_\pi$, ring) when going from the planar to the perpendicularly twisted T_1 structure, $\Delta\Delta BV(ELF_\pi$, planar−perp), reveals whether aromaticity is reduced or recovered in this process. We first examined three olefins (**1**−**3**, Scheme 1) with substituents which in the T_1 state keep the local planarity of the annulenyl rings at both the planar and $^3p^*$ olefin structures. These structures correspond to either minima or transition states on the T_1 potential energy surfaces (PESs).

In qualitative terms, the phenyl group of styrene (**1**) should be influenced by antiaromaticity at its planar T_1 olefin structure,

SCHEME 2

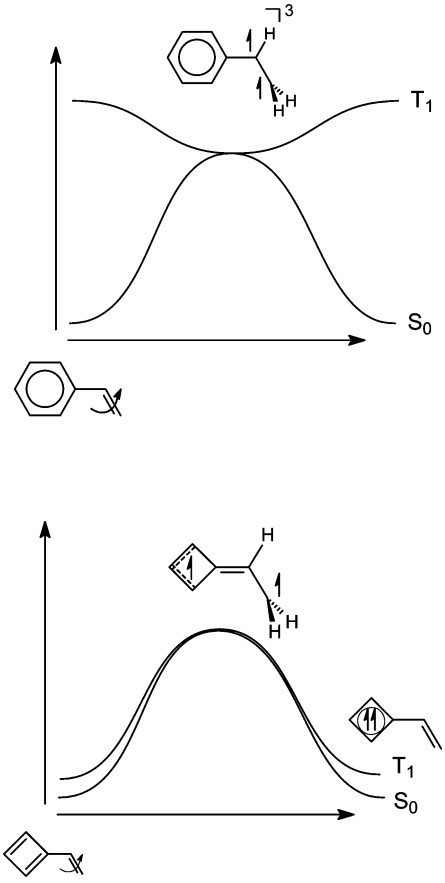

SCHEME 3

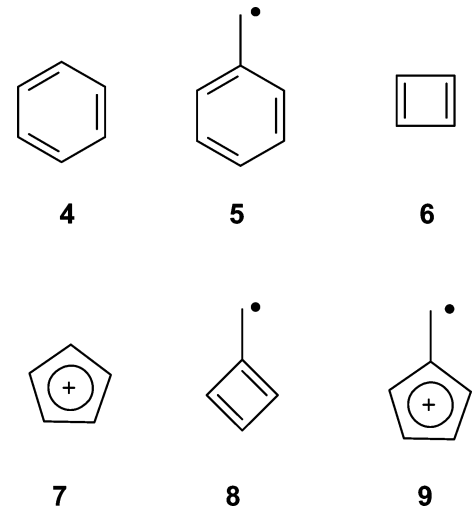

4 **5** **6**

7 **8** **9**

and when the olefin C═C bond twists to $^3p^*$, it will regain some aromatic character as a resonance structure described as an olefinic 1,2-biradical, and a closed-shell (S_0) aromatic phenyl group contributes (Scheme 2). In contrast, vinylcyclobutadiene (**2**; Scheme 2) and the vinylcyclopentadienyl cation (**3**) will in T_1 be most aromatic at the planar olefin structures, and C═C bond twist should reduce the T_1 aromatic character of the annulenyl substituents as one radical center is forced to the olefinic C_β atom. To assess the (anti)aromatic character relative to the maximum and minimum values of a certain ring type, we also computed the three annulenes **4**, **6**, and **7** (Scheme 3) in their S_0 and T_1 states, and the radicals **5**, **8**, and **9** which correspond to the methyleneannulenyl fragments of the twisted

SCHEME 4

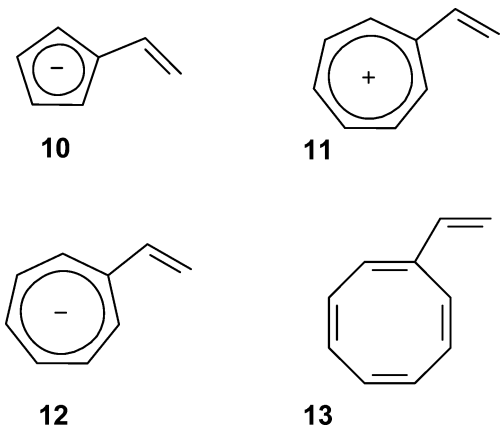

triplet olefins. Finally, we probed the T_1 aromaticity changes upon rotation about the C═C bond of the four olefins **10**−**13** (Scheme 4).

Computational Methods

All electronic structure calculations were carried out using the Gaussian 03 program package.[29] Compounds **1**−**13** were optimized at the (U)OLYP/6-311G(d,p) level of density functional theory.[30−32] The OLYP functional, in which the OPTX exchange functional is combined with the LYP correlation functional, earlier gave particularly good results for radicals.[33] Frequency calculations were performed to check the nature of the optimized structures (minima, transition states, or higher order saddle points).

The ELF was introduced by Becke and Edgecombe as a tool for topological analysis of atomic and molecular electronic structure.[34] The ELF is expressed as

$$\mathrm{ELF}(r) = [1 + (\chi_\sigma(r))^2]^{-1} = \left[1 + \left[\frac{T_\sigma(r)}{T_\sigma{}^0(r)}\right]^2\right]^{-1}$$

where χ_σ is a dimensionless localization index by which the excess local kinetic energy, $T_\sigma(r)$, due to Pauli repulsion between σ-electrons ($\sigma = \alpha$ or β) at position r is calibrated against the Thomas−Fermi kinetic energy of a uniform electron gas. With this definition, the ELF takes values in the range $0 \leq \mathrm{ELF}(r) \leq 1$, where values close (equal) to 1 are found in regions of space with strong (perfect) electron localization, and values close to 0 are found in regions with large excess kinetic energy such as in boundary regions between two electron pairs where same-spin electrons come close together. The σ- and π-components of the kinetic energy can be separated, and this also applies to the ELF, even though the sum of the two components (ELF_σ and ELF_π) does not correspond to the total ELF. To allow σ/π-separation, we kept the investigated compounds planar in their singlet and triplet states, even if these structures in a very limited number of cases correspond to transition states or higher order saddle points on the potential energy surface.

The ELFs including only the π-orbitals, giving ELF_π, were calculated with the TopMod program,[35] and the ELF isosurfaces were visualized with the VMD package.[36] As there is a gradually more rapid change in the form of isosurfaces as the ELF_π value approaches 1, we have given the ELF_π-based properties with gradually higher precision as the upper end point is approached. Moreover, in the case of the twisted triplet-state structures, the separation of Kohn−Sham orbitals into σ- and π-orbitals needs special mentioning as the π-orbitals of the ring potentially mix with the doubly occupied CH_2 fragment orbital of pseudo-π symmetry. However, in all cases except for the two cations **3** and **11**, the CH_2 fragment does not, or does only very weakly, interact with the ring and can be excluded from the ELF calculation. For **3** and **11**, the filled CH_2 fragment orbital interacts strongly with the ring orbitals and must be included. Moreover, the single electron located in the 2p(C) atomic orbital of the carbon at the CH_2 fragment of the perpendicularly twisted T_1 structure does not interact with the ring as compared to that of the planar T_1 structure. Consequently, for the neutral or anionic species this leads to ELFs based on one electron less in the twisted T_1 structure than in the planar T_1 structure, and for the cationic species **3** and **11** to ELFs based on one electron more in the twisted T_1 structure.

Optimized structures, absolute energies, symmetry, and the number of imaginary frequencies at the (U)OLYP/6-311G(d,p) level for **1**−**13** are contained in the Supporting Information.

Results and Discussion

Olefins **1**−**3** were first investigated as they previously were found to adopt C_s symmetry at all three olefin structures of interest, i.e., the planar S_0, the planar T_1, and the perpendicularly twisted T_1 (^{3}p*) structures.[16] The C_s symmetry allows for facile separation of the σ- and π-components of the ELF. These three olefins thus represent ideal systems in which the changes in aromaticity and antiaromaticity upon excitation and during a photochemical reaction can be connected to the ELF as an electronic structure property. We discuss the triplet-state properties of olefin **1** and olefins **2** and **3** separately; however, we first probed their degrees of (anti)aromaticity in S_0. The collected bifurcation values from the analysis of the ELF_π and bond length ranges of the annulenyl groups of **1**−**3** are listed in Table 1. At the end, we examined the larger olefins **10**−**13** at their planar and perpendicularly twisted structures in T_1.

Aromaticity and Antiaromaticity in S_0. The phenyl group of olefin **1** in S_0 displays a small range in the ELF_π bifurcation values ($\Delta\mathrm{BV}(\mathrm{ELF}_\pi$, ring)), the corresponding bond length alternation (Δr_{CC}(ring)) is small, the $\mathrm{RCBV}(\mathrm{ELF}_\pi$, ring) is well above 0.7, and its $\mathrm{BV}(\mathrm{ELF}_\pi$, ring) values bracket that of benzene (**4**). Consequently, in S_0 the olefinic C═C bond has only a minor influence on the aromaticity of the phenyl group of **1**. From the bifurcations in ELF_π one can see that the π-electron pairs of **1** localize marginally more to the C_2C_3, C_3C_4, and C_5C_6 bonds than the other three CC bonds of the phenyl group (Figure 1). The separation of the ELF_π basin of **1** into two basins located at the phenyl and vinyl groups, respectively, occurs at the C_1C_α bond with a $\mathrm{BV}(\mathrm{ELF}_\pi)$ of 0.411. This reveals that the conjugation between the vinyl and phenyl fragments of **1** is slightly weaker than the conjugation in 1,3-butadiene where a $\mathrm{BV}(\mathrm{ELF}_\pi)$ of 0.473 is found for the bifurcation into two vinyl basins.[5]

For olefin **2**, the $\Delta\mathrm{BV}(\mathrm{ELF}_\pi$, ring) and Δr_{CC}(ring) of the cyclobutadienyl substituent are very large and similar to those of cyclobutadiene (**6**), revealing strong antiaromaticity. From the ELF_π isosurface plots of **2** it is seen that the two π-electron pairs of the cyclobutadienyl group localize to the C_1C_2 and C_3C_4 bonds (Figure 2), and that the π-electrons of the olefin bond conjugate with the C_1C_2 bond. Thus, the π-electron pair of the C_1C_2 bond is less strongly localized than that of the C_3C_4 bond, and the conjugation with the olefin bond is stronger than in 1,3-butadiene as the bifurcation of the ELF_π basins into vinyl and C_1C_2 basins occurs at the C_1C_α bond with a $\mathrm{BV}(\mathrm{ELF}_\pi)$ of 0.656.

In **3**, the olefinic C═C bond weakens the antiaromaticity of the cyclopentadienyl ring significantly when compared to that

TABLE 1: Bifurcation Values in the Topology of the ELF$_\pi$ (BV(ELF$_\pi$, ring)), Ranges in the Bifurcation Values (ΔBV(ELF$_\pi$, ring)), and Ranges in the CC Bond Lengths (Δr_{CC}(ring)) of Annulenyl Substituents and Annulenes

compd	state, structure	symmetry, state symmetry	BV(ELF$_\pi$, ring)[a–c]	ΔBV(ELF$_\pi$, ring)	Δr_{CC}(ring)
1	S_0, planar	C_s, $^1A'$	0.857, 0.9097, 0.9056, 0.8916, 0.9224, 0.843	0.079	0.018
	T_1, planar	C_s, $^3A'$	0.487, 0.9735, 0.712, 0.799, 0.9565, 0.452	0.521	0.094
	T_1, perp	C_s, $^3A''$	0.715, 0.9354, 0.866, 0.870, 0.9332, 0.720	0.220	0.042
2	S_0, planar	C_s, $^1A'$	0.9864, 0.149, 0.999336, 0.07	0.93	0.244
	T_1, planar	C_s, $^3A'$	0.475, 0.779, 0.738, 0.486	0.304	0.045
	T_1, perp	C_s, $^3A''$	0.324, 0.835, 0.834, 0.331	0.511	0.077
3	S_0, planar	C_s, $^1A'$	0.693; 0.9946, 0.181, 0.9990, 0.271	0.818	0.175
	T_1, planar	C_s, $^3A'$	0.688, 0.795, 0.9133, 0.793, 0.681	0.232	0.038
	T_1, perp	C_s, $^3A''$	0.587, 0.869, 0.9234, 0.877, 0.554	0.369	0.053
4, C_6H_6	S_0	D_{6h}, $^1A_{1g}$	0.9068, 0.9068, 0.9068, 0.9068, 0.9068, 0.9068	0.000	0.000
	T_1	D_{2h}, $^3B_{1u}$	0.8892, 0.144, 0.8892, 0.8892, 0.144, 0.8892	0.745	0.129
5	D_0	C_{2v}, $^2B_1$	0.714, 0.9361, 0.8657, 0.8657, 0.9361, 0.714	0.222	0.044
6, C_4H_4	S_0	D_{2h}, ^1A_g	0.999715, 0.09, 0.999715, 0.09	0.91	0.239
	T_1	D_{4h}, $^3A_{1g}$	0.651, 0.651, 0.651, 0.651	0.000	0.000
7, $C_5H_5^+$	S_0	C_{2v}, $^1A_1$	0.726, 0.999774, 0.04, 0.999774, 0.726	0.96	0.226
	T_1	D_{5h}, $^3A_1'$	0.8166, 0.8166, 0.8166, 0.8166, 0.8166	0.000	0.000
8	D_0	C_{2v}, $^2A_2$	0.319, 0.839, 0.839, 0.319	0.520	0.079
9	D_0	C_{2v}, $^2A_2$	0.525, 0.8989, 0.9136, 0.8989, 0.525	0.389	0.049

[a] BV(ELF$_\pi$, ring) values <0.10 are given with two decimals, BV(ELF$_\pi$, ring) values in the range 0.10 < BV(ELF$_\pi$, ring) ≤ 0.85 are given with three decimals, those in the range 0.85 < BV(ELF$_\pi$, ring) ≤ 0.95 are given with four decimals, and BV(ELF$_\pi$, ring) values >0.95 are given with five decimals (or more). [b] Ring closure bifurcation values are underlined. [c] The atoms are numbered as in Scheme 1.

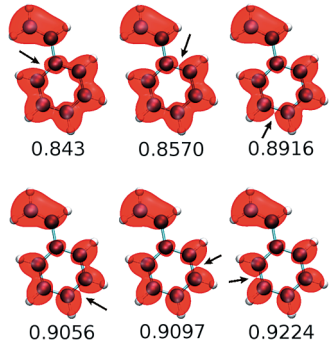

Figure 1. Isosurface plots of the π-contribution to the electron localization function (ELF$_\pi$) of **1** in the S_0 state at the values at which bifurcations in the basins take place. BV(ELF$_\pi$) values of <0.85 are given with three decimals, and those in the range 0.85 < BV(ELF$_\pi$) ≤ 0.95 are given with four decimals. Arrows point to the bonds where the bifurcations occur.

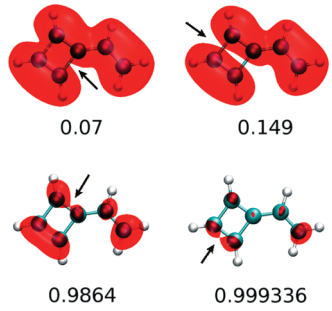

Figure 2. Isosurface plots of the π-contribution to the electron localization function of **2** in the S_0 state at the values at which bifurcations in the basins take place. BV(ELF$_\pi$) values below 0.10 are given with two decimals, those in the range 0.10 < BV(ELF$_\pi$) ≤ 0.85 are given with three decimals, those in the range 0.85 < BV(ELF$_\pi$) ≤ 0.95 are given with four decimals, and BV(ELF$_\pi$) values >0.95 are given with five or more decimals. Arrows point to the bonds where the bifurcations occur.

of the cyclopentadienyl cation (**7**), as revealed by the lower ΔBV(ELF$_\pi$, ring) and Δr_{CC}(ring) of **3**. The RCBV(ELF$_\pi$, ring) of **3** vs that of **7** supports this interpretation, and the BV(ELF$_\pi$) at the C_1C_α bond in **3** (0.877) confirms the strong π-interaction between the ring and olefin fragments. Hence, the π-electron system of **3** can be described as composed of a *cis*-butadiene and an allyl cationic fragment. Taken together, the stronger π-interactions between the olefin and annulenyl fragments in **2** and **3** than in **1** are reflected in the BV(ELF$_\pi$) values for the basin separations at the C_1C_α bonds.

Styrene (1) in the T_1 State. At the planar T_1 structure of **1**, which corresponds to the transition state for rotation about the C═C bond, the ΔBV(ELF$_\pi$, ring) is significantly larger than in S_0, revealing that the phenyl substituent is now nonaromatic or antiaromatic. The lowering of the RCBV(ELF$_\pi$, ring) upon excitation to T_1 is apparent, even though it is well above the RCBV(ELF$_\pi$) of benzene (**4**) in T_1. This last fact shows that the olefinic C═C bond lowers the T_1 antiaromaticity of the benzene ring, as observed for **3** in S_0, where the cyclopentadienyl antiaromaticity is lower than that of **7**. Evidence for the strong vinyl−phenyl π-interaction in **1** is given by the BV(ELF$_\pi$) of 0.9360 and 0.440 for the basin separations at the C_1C_α and $C_\alpha C_\beta$ bonds in the planar T_1 structure. On the basis of the BV(ELF$_\pi$), π-electron pair localization is thus most apparent to the C_2C_3, C_5C_6, and C_1C_α bonds (Figure 3) in agreement with a quinoid-type resonance structure (Scheme 5), such as earlier also found by Bearpark et al. at the CASSCF level.[37] Strong vinyl−annulenyl group interaction as a mode for reduction of antiaromatic character is therefore found in S_0 for olefins with $4n$ π-electron substituents and in T_1 for olefins with $4n + 2$ π-electron substituents.

At the ^{3}p* structure of **1**, the triplet biradical character will to a larger extent than in the planar T_1 structure be localized to the olefinic C═C bonds (Figure 4). Consequently, the T_1 antiaromatic character of the phenyl group is reduced as resonance structures with the triplet biradical localized to the twisted olefin bond allow the phenyl group to regain part of its S_0 (closed-shell) aromaticity. Accordingly, when the C═C bond of **1** is twisted in the T_1 state, the ΔBV(ELF$_\pi$, ring) decreases considerably, leading to a ΔΔBV(ELF$_\pi$, planar−perp) of 0.30. The RCBV(ELF$_\pi$, ring) also becomes higher, and the regain in aromaticity upon C═C bond twist in **1** in the T_1 state is reflected in an energy reduction of 6.2 kcal/mol, somewhat lower than the experimental values (9.6−13.7 kcal/mol).[38,39] From comparison with the benzyl radical **5**, it is clear that the phenyl group of styrene at its ^{3}p* structure is aromatic to a degree

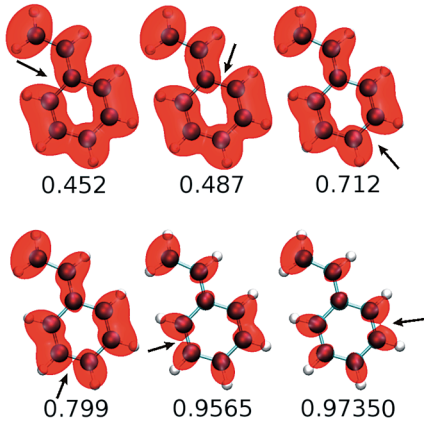

Figure 3. Isosurface plots of the π-contribution to the electron localization function of **1** at its planar T_1 structure at the values at which bifurcations in the basins occur. $BV(ELF_\pi)$ values in the range $0.10 < BV(ELF_\pi) \leq 0.85$ are given with three decimals, those in the range $0.85 < BV(ELF_\pi) \leq 0.95$ are given with four decimals, and $BV(ELF_\pi)$ values >0.95 are given with five decimals. Arrows point to the bonds where the bifurcations occur.

SCHEME 5

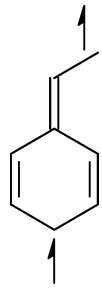

similar to that of **5**. Thus, the ELF_π properties as aromaticity measures directly linked to electronic structure verify that a change in aromatic character correlates with the T_1 PES profile of **1**.

Olefins 2 and 3 in the T_1 States. At the planar T_1 geometries of **2** and **3**, which are minima on the PES, the $4n\pi$-electron rings are influenced by triplet-state aromaticity. This increase in aromatic character upon excitation from S_0 to T_1 is reflected

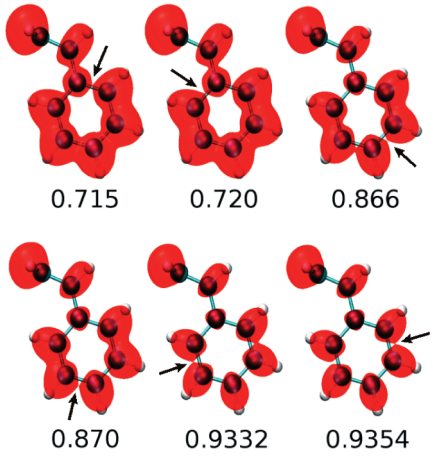

Figure 4. Isosurface plots of the π-contribution to the electron localization function of **1** at its perpendicularly twisted T_1 structure at values at which bifurcations in the basins occur. $BV(ELF_\pi)$ values in the range $0.10 < BV(ELF_\pi) \leq 0.85$ are given with three decimals, and those in the range $0.85 < BV(ELF_\pi) \leq 0.95$ are given with four decimals. Arrows point to the bonds where the bifurcations occur.

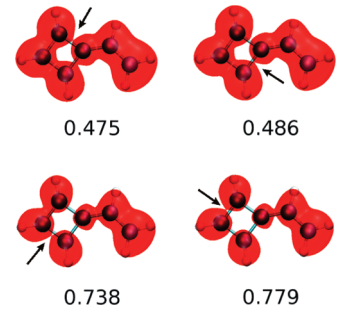

Figure 5. Isosurface plots of the π-contribution to the electron localization function of **2** at its planar T_1 structure at the values at which bifurcations in the basins occur. $BV(ELF_\pi)$ values in the range $0.10 < BV(ELF_\pi) \leq 0.85$ are given with three decimals. Arrows point to the bonds where the bifurcations occur.

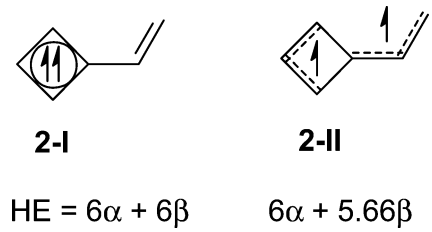

Figure 6. Resonance structure descriptions of the π-system of **2** at its planar T_1 structure as either a triplet biradical cyclobutadiene plus an olefinic C=C bond (**2-I**) or two separated allyl radicals (**2-II**). The energies of the two triplet biradical resonance structures according to Hückel MO theory are given. Note that according to Hückel MO theory the energy of a triplet biradical is equal to that of the corresponding open-shell singlet biradical.

in significant reductions in $\Delta BV(ELF_\pi, \text{ring})$, yet both olefins at their planar T_1 structures display nonzero $\Delta BV(ELF_\pi, \text{ring})$ in contrast to the corresponding annulenes **6** and **7**. The reductions in $\Delta BV(ELF_\pi, \text{ring})$ of **2** and **3** upon excitation to T_1 are also large, but the $\Delta BV(ELF_\pi, \text{ring})$ of the phenyl group of **1** in S_0 is still smaller. The $RCBV(ELF_\pi, \text{ring})$ values of **2** and **3** are substantially lower than those of **6** and **7**, and lower than our threshold of 0.7 for an aromatic compound. There are also CC bond length variations in the rings of the planar T_1 structures of **2** and **3**, even though these are modest. Consequently, the cyclobutadienyl ring of **2** and the cyclopentadienyl cationic ring of **3** in T_1 are best classified as nonaromatic, and this agrees with our previous finding of NICS(0) values which are close to 0,[16] indicating nonaromaticity. The HOMA values of **2** and **3** calculated at OLYP/TZ2P (0.033 and 0.553) differed significantly, a possible result of both weaker π-bonding and bond angle strain in the four-membered ring of **2**, leading to longer CC bonds and a large deviation from the HOMA reference CC bond length of an aromatic compound (1.388 Å).

From the plots of ELF_π it is seen that the π-system of planar triplet biradical **2** dissects into two allyl radicals (Figure 5), in line with the earlier finding by Borden and Davidson that the two NBMOs of biradical **2** can be confined to two different sets of atoms.[40] Even though the Hückel energies for the two idealized biradical resonance structures **2-I** and **2-II** (Figure 6) are in favor of the T_1 aromatic description **2-I**, the energy difference is modest and the cyclobutadienyl ring of **2** is not influenced by T_1 aromaticity to the same extent as cyclobutadiene (**6**). Here it should be noted that Hückel MO theory, according to which the triplet biradical is of the same energy as the corresponding open-shell singlet biradical, provides only a rough estimate.

When twisted about the olefinic C=C bond, the aromatic character of the rings of **2** and **3** clearly decreases as the

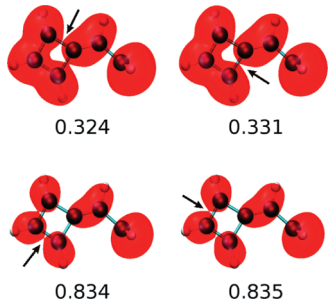

Figure 7. Isosurface plots of the π-contribution to the electron localization function of **2** at its perpendicularly twisted T_1 structure at values where bifurcations in the basins occur. BV(ELF$_\pi$) values in the range $0.10 < \text{BV(ELF}_\pi) \leq 0.85$ are given with three decimals. Arrows point to the bonds where the bifurcations occur.

ΔBV(ELF$_\pi$, ring) values increase and the RCBV(ELF$_\pi$, ring) values become lower (Figure 7). In contrast to **1**, where a positive $\Delta\Delta$BV(ELF$_\pi$, planar−perp) was observed, negative $\Delta\Delta$BV(ELF$_\pi$, planar−perp) values of −0.21 and −0.14 are found for **2** and **3**, respectively. The Δr_{CC}(ring) values increase, but they are still much lower than those of **2** and **3** in S_0. Both ΔBV(ELF$_\pi$, ring) and Δr_{CC}(ring) approach closely the values of the radicals **8** and **9** (Table 1), so that the extent of substituent antiaromaticity is modest. The loss of T_1-state aromaticity is reflected in activation barriers of 21.6 and 27.1 kcal/mol for the twists about the C═C bonds in **2** and **3**. At the CASPT2/[4s3p2d/3s1p]//CASSCF/[4s3p2d/3s1p] level the barrier of **2** was previously calculated at 24.3 kcal/mol.[16] Although **2** in T_1 can be described as two allyl radicals, the rotational barrier of the olefin bond is higher than the CC rotational barrier of the allyl radical (17.3 kcal/mol with UOLYP/6-311G(d,p)), revealing a higher $C_\alpha C_\beta$ bond order in **2** than in the allyl radical, in line with partial influence of the aromatic resonance structure **2-I**.

It should be noted that large differences between the ΔHOMA(planar−perp) and ΔNICS(planar−perp) of **2** and **3** were previously observed. The ΔHOMA(planar−perp) revealed a significant decrease in aromaticity for **2** but a negligible change for **3**, whereas ΔNICS(planar−perp) revealed the opposite, a very large reduction in aromaticity upon C═C bond twist for **3** and a much smaller one for **2**.[16] The $\Delta\Delta$BV(ELF$_\pi$, planar−perp), as an electronic structure based index, reveals a significant reduction in aromaticity for both olefins, however a somewhat smaller reduction for **3**.

Other Annulenyl-Substituted Olefins. We also examined olefins **10**−**13**, the first two of which have annulenyl substituents with six π-electrons and the last two have substituents with eight π-electrons. We only investigated these olefins in their T_1 states because two of them (**12** and **13**) are markedly puckered in S_0. In T_1 we constrained them to C_s symmetry, even though the vinyl group of **13** is slightly twisted out-of-plane of the COT ring at its optimal T_1 geometry (C−C−C═C dihedral angles at −169.0 and 12.0°). The largest difference in CC bond lengths between the optimal nonplanar and the C_s symmetric structure is merely 0.0005 Å, and the energy difference is 0.01 kcal/mol.

In their planar T_1 structures, **10** and **11** should be categorized as nonaromatic rather than antiaromatic on the basis of ΔBV(ELF$_\pi$, ring), $\Delta\Delta$BV(ELF$_\pi$, planar−perp), and RCBV(ELF$_\pi$, ring). One can also note that the vinyl group lowers the antiaromaticity of the annulenyl rings significantly because ΔBV(ELF$_\pi$) values of 0.707 and 0.831 were found for $C_5H_5^-$ and $C_7H_7^+$ in their T_1 states, to be compared with 0.370 and 0.520 of **10** and **11**. Upon C═C bond twist, ΔBV(ELF$_\pi$) and RCBV(ELF$_\pi$, ring) reveal regained influence of aromaticity (Table 2), but the values are slightly smaller than those observed for styrene. The energy lowerings upon a twist of the C═C bonds of **10** and **11** are 2.0 and 1.3 kcal/mol respectively, and their $\Delta\Delta$BV(ELF$_\pi$, planar−perp) values are smaller than for **1** (0.15 and 0.24 for **10** and **11**, respectively, and 0.30 for **1**, Tables 1 and 2). The same trend in relative aromaticity recovery in T_1 among **1**, **10**, and **11** was earlier observed with HOMA, but with NICS(0) it was found that **11** regained most aromaticity upon C═C bond rotation.[16]

In contrast, olefins **12** and **13** with eight π-electron substituents are significantly influenced by aromaticity at the planar optimal T_1 structures as the ΔBV(ELF$_\pi$, ring) values of these structures are small. They also display the same trend in $\Delta\Delta$BV(ELF$_\pi$, planar−perp) as **2** and **3** with negative values (−0.19 and −0.32, respectively), and ^{3}p* structures of **12** and **13** are 32.2 and 28.3 kcal/mol higher in energy than the planar ones. Noteworthy, the Hückel energy difference between the two idealized resonance structures **13-I** and **13-II** (Figure 8) is large and in favor of the T_1 aromatic **13-I**. Interestingly, the increased importance of this T_1 aromatic structure when compared to **2** is reflected in both the higher energy barrier for C═C bond twist and a more negative $\Delta\Delta$BV(ELF$_\pi$, planar−perp) for **13**. A larger reduction in aromaticity upon C═C bond twist in **13** than in **12** was also found with HOMA, whereas the changes in NICS(0) were more equal.[16] Thus, the ELF$_\pi$ properties as aromaticity indicators directly linked to electronic structure reveal that olefins with COT substituents, such as

TABLE 2: Bifurcation Values in the Topology of the ELF$_\pi$ (BV(ELF$_\pi$, ring)), Ranges in the Bifurcation Values (ΔBV(ELF$_\pi$, ring)), and Ranges in the CC Bond Lengths (Δr_{CC}(ring)) of Annulenyl Substituents of Olefins 10−13

olefin	state, structure	symmetry, state symmetry	BV(ELF$_\pi$, ring)[a−c]	ΔBV(ELF$_\pi$, ring)	Δr_{CC}(ring)
10	T_1, planar[d]	C_s, ^{3}A′	0.573, 0.873, 0.684, 0.876, 0.506	0.370	0.140
	T_1, perp[d]	C_s, ^{3}A″	0.653, 0.8765, 0.752, 0.8713, 0.669	0.223	0.047
11	T_1, planar	C_s, ^{3}A′	0.630, 0.9703, 0.757, 0.9646, 0.712, 0.98675, 0.467	0.520	0.086
	T_1, perp	C_s, ^{3}A″	0.706, 0.9746, 0.840, 0.9643, 0.838, 0.9761, 0.695	0.281	0.052
12	T_1, planar	C_s, ^{3}A′	0.641, 0.827, 0.816, 0.726, 0.841, 0.795, 0.677	0.200	0.036
	T_1, perp	C_s, ^{3}A″	0.479, 0.869, 0.831, 0.751, 0.855, 0.823, 0.559	0.390	0.062
13	T_1, planar[e]	C_s, ^{3}A′	0.738, 0.898, 0.812, 0.872, 0.851, 0.829, 0.895, 0.729	0.169	0.032
	T_1, perp	C_s, ^{3}A″	0.465, 0.9603, 0.749, 0.888, 0.885, 0.754, 0.9591, 0.466	0.495	0.085

[a] BV(ELF$_\pi$, ring) values <0.10 are given with two decimals, BV(ELF$_\pi$, ring) values in the range $0.10 < \text{BV(ELF}_\pi\text{, ring)} \leq 0.85$ are given with three decimals, those in the range $0.85 < \text{BV(ELF}_\pi\text{, ring)} \leq 0.95$ are given with four decimals, and BV(ELF$_\pi$, ring) values >0.95 are given with five decimals or more. [b] Ring closure bifurcation values are underlined. [c] The atoms are numbered as in Scheme 4. [d] Olefin **10** contains an extra imaginary frequency corresponding to an out-of-plane deformation of the ring in both planar and twisted double bonds. [e] Contains one out-of-plane imaginary frequency.

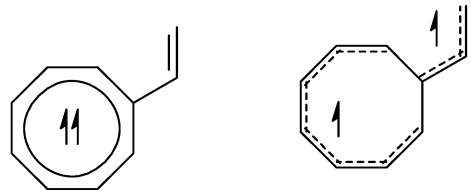

13-I **13-II**

HE = 10α + 11.96β 10α + 10.88β

Figure 8. Resonance structure descriptions of **13** at its planar T_1 structure as either a triplet biradical cyclooctatetraene plus an olefinic C═C bond (**13-I**) or an allyl radical plus a heptatrienyl radical (**13-II**). The energies of the two triplet biradical resonance structures according to Hückel MO theory are given. Note that according to Hückel MO theory the energy of a triplet biradical is equal to that of the corresponding open-shell singlet biradical.

bisstyrylcyclooctatetraene,[28] have exceptionally high rotational barriers as a result of the loss in aromaticity in this process.

Conclusions

The π-contribution to the electron localization function (ELF_π) confirms that there is a distinct connection between aromaticity changes of the annulenyl groups of substituted olefins and the shapes of their T_1 potential energy surfaces for rotation about the C═C bond. The lowest point on the T_1 PES investigated here corresponds to the structure with the highest degree of aromaticity. This implies that triplet-state (excited-state) $4n$ π-electron aromaticity is a feature that influences photochemical reactions, as $4n + 2$ π-electron aromaticity influences many reactions in the electronic ground state. By tuning the degree of excited-state aromaticity of the substituents at an olefin, one should be able to predictably tune the shape of the T_1 PES so that it meets requirements for, e.g., optimal behavior as an optical switch.

Acknowledgment. We are grateful to the Carl Trygger Foundation for a postdoctoral fellowship to S.V. and to the National Supercomputer Centre in Linköping, Sweden, for a generous allotment of computer time.

Supporting Information Available: Listing of optimized structures, absolute energies, symmetry, and number of imaginary frequencies at the (U)OLYP/6-311G(d,p) level for **1**−**13**. This material is available free of charge via the Internet at http://pubs.acs.org.

References and Notes

(1) Minkin, V. I.; Glukhovtsev, M. N.; Simkin, B. Ya. *Aromaticity and Antiaromaticity: Electronic and Structural Aspects*; Wiley Interscience: New York, 1994.
(2) See the special issue on aromaticity: Schleyer, P. v. R., Ed. *Chem. Rev.* **2001**, *101*, 1115.
(3) Baird, N. C. *J. Am. Chem. Soc.* **1972**, *94*, 4941.
(4) Gogonea, V.; Schleyer, P. v. R.; Schreiner, P. R. *Angew. Chem., Int. Ed.* **1998**, *37*, 1945.
(5) Villaume, S.; Fogarty, H. A.; Ottosson, H. *ChemPhysChem* **2008**, *9*, 257.
(6) Soncini, A.; Fowler, P. W. *Chem. Phys. Lett.* **2008**, *450*, 431.
(7) Zilberg, S.; Haas, Y. *J. Phys. Chem. A* **1998**, *102*, 10843.
(8) (a) Garavelli, M.; Bernardi, F.; Moliner, V.; Olivucci, M. *Angew. Chem., Int. Ed.* **2001**, *40*, 1466. (b) Garavelli, M.; Bernardi, F.; Cembran, A.; Caslao, O.; Frutos, L. M.; Merchan, M.; Olivucci, M. *J. Am. Chem. Soc.* **2002**, *124*, 13770.
(9) Karadakov, P. B. *J. Phys. Chem. A* **2008**, *112*, 7303.
(10) Karadakov, P. B *J. Phys. Chem. A* **2008**, *112*, 12707.
(11) (a) Balkova, A.; Bartlett, R. J. *J. Chem. Phys.* **1994**, *101*, 8972. (b) Koseki, S.; Toyota, A. *J. Phys. Chem. A* **1997**, *101*, 5712.
(12) Möllerstedt, H.; Piqueras, M. C.; Crespo, R.; Ottosson, H. *J. Am. Chem. Soc.* **2004**, *126*, 13938.
(13) Ottosson, H.; Kilså, K.; Chajara, K.; Piqueras, M. C.; Crespo, R.; Kato, H.; Muthas, D. *Chem.—Eur. J.* **2007**, *13*, 6998.
(14) Brink, M.; Möllerstedt, H.; Ottosson, C.-H. *J. Phys. Chem. A* **2001**, *105*, 4071.
(15) Krygowski, T. M. *J. Chem. Inf. Comput. Sci.* **1993**, *33*, 70.
(16) Kato, H.; Brink, M.; Möllerstedt, H.; Piqueras, M. C.; Crespo, R.; Ottosson, H. *J. Org. Chem.* **2005**, *70*, 9495.
(17) Feixas, F.; Matito, E.; Poater, J.; Solà, M. *J. Comput. Chem.* **2008**, *29*, 1543.
(18) Giambiagi, M.; de Giambiagi, M. S.; dos Santos, C. D.; de Figueiredo, A. P. *Phys. Chem. Chem. Phys.* **2000**, *2*, 3381.
(19) Cioslowski, J.; Matito, E.; Solà, M. *J. Phys. Chem. A* **2007**, *111*, 6521.
(20) Bultinck, P.; Rafat, M.; Ponec, R.; van Gheluwe, B.; Carbó-Dorca, R.; Popelier, P. *J. Phys. Chem. A* **2006**, *110*, 7642.
(21) (a) Poater, J.; Fradera, X.; Duran, M.; Solà, M. *Chem.—Eur. J.* **2003**, *9*, 400. (b) Poater, J.; Fradera, X.; Duran, M.; Solà, M. *Chem.—Eur. J.* **2003**, *9*, 1113.
(22) Matito, E.; Duran, M.; Solà, M. *J. Chem. Phys.* **2005**, *122*, 014109; erratum **2006**, *125*, 059901.
(23) Matito, E.; Feixas, F.; Solà, M. *J. Mol. Struct.: THEOCHEM* **2007**, *811*, 3.
(24) Santos, J. C.; Tiznado, W.; Contreras, R.; Fuentealba, P. *J. Chem. Phys.* **2004**, *120*, 1670.
(25) Malrieu, J.-P.; Lepetit, C.; Gicquel, M.; Heully, J.-L.; Fowler, P. W.; Chauvin, R. *New J. Chem.* **2007**, *31*, 1918.
(26) Santos, J. C.; Andres, J.; Aizman, A.; Fuentealba, P. *J. Chem. Theory Comput.* **2005**, *1*, 83.
(27) For reviews see, e.g.: (a) Waldeck, D. H. *Chem. Rev.* **1991**, *91*, 415. (b) Arai, T.; Tokumaru, T. *Chem. Rev.* **1993**, *93*, 23. (c) Goerner, H.; Kuhn, H.-J. *Adv. Photochem.* **1995**, *1*, 19.
(28) Anger, I.; Sundahl, M.; Wennerström, O.; Auchter-Krummel, P.; Müllen, K. *J. Phys. Chem.* **1995**, *99*, 650.
(29) Frisch, M. J.; Trucks, G. W.; Schlegel, H. B.; Scuseria, G. E.; Robb, M. A.; Cheeseman, J. R.; Montgomery, J. A., Jr.; Vreven, T.; Kudin, K. N.; Burant, J. C.; Millam, J. M.; Iyengar, S. S.; Tomasi, J.; Barone, V.; Mennucci, B.; Cossi, M.; Scalmani, G.; Rega, N.; Petersson, G. A.; Nakatsuji, H.; Hada, M.; Ehara, M.; Toyota, K.; Fukuda, R.; Hasegawa, J.; Ishida, M.; Nakajima, T.; Honda, Y.; Kitao, O.; Nakai, H.; Klene, M.; Li, X.; Knox, J. E.; Hratchian, H. P.; Cross, J. B.; Bakken, V.; Adamo, C.; Jaramillo, J.; Gomperts, R.; Stratmann, R. E.; Yazyev, O.; Austin, A. J.; Cammi, R.; Pomelli, C.; Ochterski, J. W.; Ayala, P. Y.; Morokuma, K.; Voth, G. A.; Salvador, P.; Dannenberg, J. J.; Zakrzewski, V. G.; Dapprich, S.; Daniels, A. D.; Strain, M. C.; Farkas, O.; Malick, D. K.; Rabuck, A. D.; Raghavachari, K.; Foresman, J. B.; Ortiz, J. V.; Cui, Q.; Baboul, A. G.; Clifford, S.; Cioslowski, J.; Stefanov, B. B.; Liu, G.; Liashenko, A.; Piskorz, P.; Komaromi, I.; Martin, R. L.; Fox, D. J.; Keith, T.; Al-Laham, M. A.; Peng, C. Y.; Nanayakkara, A.; Challacombe, M.; Gill, P. M. W.; Johnson, B.; Chen, W.; Wong, M. W.; Gonzalez, C.; Pople, J. A. *Gaussian 03*, revision D.01; Gaussian, Inc.: Pittsburgh, PA, 2001.
(30) Handy, N. C.; Cohen, A. *J. Mol Phys.* **2001**, *99*, 403. (b) Hoe, W.-M.; Cohen, A. J.; Handy, N. C *Chem. Phys. Lett.* **2001**, *341*, 319.
(31) Lee, C.; Yang, W.; Parr, R. G. *Phys. Rev. B* **1988**, *37*, 785.
(32) Krishnan, R.; Binkley, J. S.; Seeger, R.; Pople, J. A. *J. Chem. Phys.* **1980**, *72*, 650.
(33) Baker, J.; Pulay, P. *J. Chem. Phys.* **2002**, *117*, 1441.
(34) Becke, A. D.; Edgecombe, K. E. *J. Chem. Phys.* **1990**, *92*, 5397.
(35) Noury, S.; Krokidis, K.; Fuster, F.; Silvi, B. *TopMoD Package*; Université Pierre et Marie Curie: Paris, 1997.
(36) VMD—Visual Molecular Dynamics: Humphrey, W.; Dalke, A.; Schutten, K. *J. Mol. Graphics* **1996**, *14*, 33.
(37) Bearpark, M. J.; Olivucci, M.; Wilsey, S.; Bernardi, F.; Robb, M. A. *J. Am. Chem. Soc.* **1995**, *117*, 6944.
(38) Ni, T.; Caldwell, R. A.; Melton, L. A. *J. Am. Chem. Soc.* **1989**, *111*, 457.
(39) Evans, D. *J. Chem. Soc.* **1957**, 1351.
(40) Borden, W. T.; Davidson, E. R. *J. Am. Chem. Soc.* **1977**, *99*, 4587.

JP904335J